Design and Characterization of a 60 GHz Low-Noise Amplifier in GaAs m-HEMT Technology for Radar Detection Systems

Pape Sanoussy Diao, Thierry Alves, Benoit Poussot and Martine Villegas

ESYCOM, Univ Gustave Eiffel, CNRS UMR 9007, F-77454 Marne-la-Vallée, France
Email: pape-sanoussy.diao@esiee.fr, thierry.alves@esiee.fr

***Abstract*—This paper addresses the design of a 60 GHz low-noise amplifier for radar detection systems. Based on an impulse architecture, the required characteristics of the amplifier are determined to improve the system performance, especially in terms of range. The choice of the design technology is based on a detailed comparative study. Then, the amplifier is designed in a 70 nm gallium-arsenide metamorphic high electron mobility transistor technology. It includes three-stages transistors with inductive degeneration for a suitable trade-off between gain and noise. Critical design points related to coupling phenomena are identified in the layout realization. To limit these coupling effects, a progressive optimization method is used. The optimized amplifier achieves a gain of 14.3 dB and a noise factor of 2.1 dB at 60 GHz. The simulated non-linear characteristics show an input 1 dB compression point $IP_{1dB} = -9.6$ dBm and an input third-order intercept point $IIP3 \approx -4$ dBm. A good impedance matching at the input ($S_{11} < -15.4$ dB) and the output ($S_{22} < -16.3$ dB) is obtained in the frequency band of interest. The designed circuit consumes a total direct current power of 13.5 mW and occupies an area of 1.47×1.0 mm^2. In addition, the sensitivity characterization of the amplifier to voltage biasing, temperature and input impedance variations shows a good robustness of the design.**

Keywords–LNA design and characterization; 60 GHz; GaAs m-HEMT; Radar detection systems; Millimeter-wave technology.

I. Introduction

A 60 GHz Low-Noise Amplifier (LNA) has been concisely proposed in [1] for multi-band impulse detection system. But, for a more complete study, background, technology choice and design methodology need to be more detailed. In addition, the design characterization should be done taking into account the architecture considered and the targeted performance. This present study is motivated by the aforementioned reasons to bring a further development of the work presented in [1].

Availability of unlicensed bandwidth around 60 GHz in several regions of the world (57-66 GHz in Europe [2]) generates great interest in the development of new wireless systems. In radar, the use of millimeter-wave frequencies is often preferred to facilitate the detection of small objects (for example, bullets whose largest dimension does not exceed 10 cm). Furthermore, large bandwidths allow to achieve high spatial resolutions (a few cm). But, the use of millimeter-wave frequencies faces challenges related to the design, realization and even packaging of components. However, in recent decades, standards developments in millimeter-wave bands have contributed to significant advances in terms of integrated circuit technologies. For example, new process in Silicon-Germanium (SiGe) [3] [4] and III-V materials [5] [6] technologies allow the production of devices and systems for a variety of applications in millimeter-wave bands. These opportunities create a need for increasingly high-performance devices. In this context, this study adresses the design of a LNA with moderate gain and low power consumption, which has relatively wide bandwidth and small size in order to improve the performance of radar detection systems.

More generally, this work is part of a large study on the development of an ultra-wideband millimeter-wave detection system combining simplicity in terms of architecture and signal processing, low power consumption and small size. The objective is then to detect metal objects such as cylinders and plates, over short ranges (a few meters). In this study, the considered detection context is the monostatic radar configuration as described in Figure 1, where the target is a cylindrical metal of radius r and height h $(r; h)$. The detection system is schematized by a transceiver (TX-RX) using the same antenna, but it can also use two co-located antennas. The incidence angle θ indicates the orientation of the target with respect to the antenna boresight.

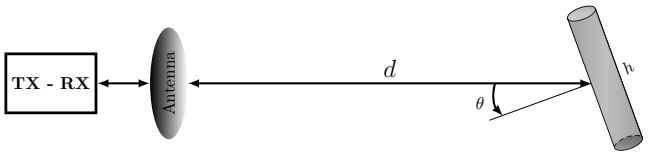

Figure 1. Context of the detection.

This contribution proposes the design and characterization of a LNA in a 70 nm Gallium-Arsenide (GaAs) metamorphic High Electron Mobility Transistor (m-HEMT) technology. It is organized as follows: Section II presents the detection principle and the associated architecture. In Section III the sizing of the proposed system is presented and the specifications of the LNAs are determined. Based on a detailed comparison, the design technology is chosen and described in Section IV. Then, the design principle is presented in Section V. In Section VI, we present the layout realization and electromagnetic simulations results. Design optimization and characterization are highlighted in Section VII. In addition, results are discussed and a comparison with the state-of-the-art is presented. And finally, a conclusion and future work are addressed in Section VIII.

II. Principle of the Detection

The angular dependence of the Radar Cross Section (RCS) of typical targets such as cylinders and plates (see Figure 2)

often results in a limitation of the detection range, particularly when they rotate away from the normal incidence. RCSs shown in Figure 2 are obtained from an electromagnetic simulation software called High Frequency Structure Simulator (HFSS). This limitation of the detection range occurs even when targets are close to the radar system and depends on their dimensions according to the operating wavelength [7]. To overcome this limitation, we use frequency diversity [8]. The idea is to take advantage of the frequency channel diversity due to the frequency dependence of the target RCS. This dependency is illustrated in Figure 3 with RCS simulations from HFSS for the normal incidence. Note that this frequency dependence of the RCSs may be more or less strong depending on the angle of incidence.

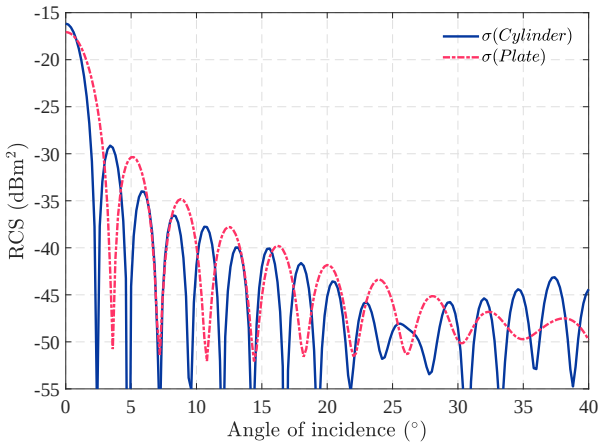

Figure 2. RCS of metallic targets as a function of elevation angle for cylinder (0.6 cm; 6 cm) and azimut angle for plate (0.5×4 cm^2) at 60 GHz.

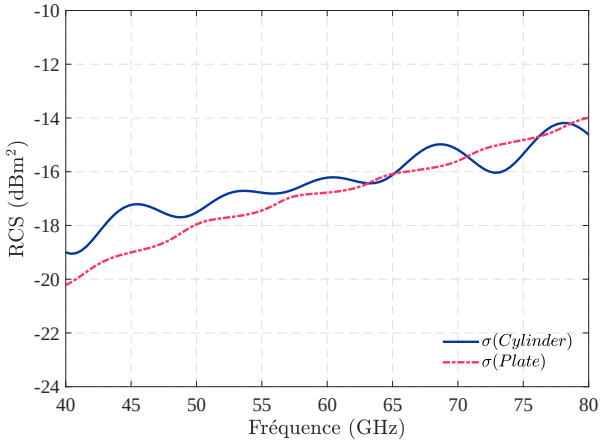

Figure 3. RCS of metallic targets as a function of frequency for cylinder (0.6 cm; 6 cm) and plate (0.5×4 cm^2) in normal incidence.

The proposed detection principle is then based on the impulse technique, using a multi-band approach [7] [9], to improve detection coverage, particularly the continuity of detection according to the target orientation angle θ. Frequencies around 60 GHz are chosen for spectrum availability [2], and also for their short wavelengths (5 mm at 60 GHz) to detect small objects, i.e., those whose largest dimension $\leq$ 10 cm.

The architecture associated with the detection principle is shown in Figure 4 in the case of a dual-band system around frequencies 57.8 GHz and 62.8 GHz. In the transmitter, Differential Structure Power Amplifiers (DSPAs), whose operation is based on the even mode rejection are used. DSPA$_1$ provides both signal division and pre-amplification. The signals selected by the filter bank are then amplified by DSPA$_2$ and transmitted by the same antenna. In reception, simple LNAs are used for better noise performance. The received signals are selected by a filter bank identical to the one in transmission before being subjected to the detection and decision process. More details of the architecture operation are given in [9].

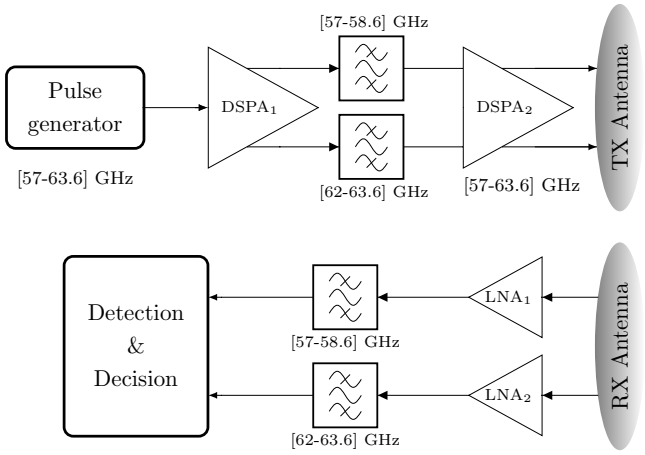

Figure 4. Dual-band detection architecture.

The proposed architecture can be applied in a more general case with N frequency bands. It has advantages in terms of simplicity of implementation by using impulse technique and does not required any frequency conversion. The processing of the received signals can be done by different techniques: selection combining, cumulative detection [9], coherent integration or non-coherent integration [10]. All of these techniques can help to improve the performance in terms of detection range compared to a single frequency band system.

III. Required Specifications of the LNA

To determine the specifications of the LNA, a full system sizing must be performed. For this, we start from the monostatic radar equation giving the maximum detection range (R_{max}) as a function of the minimum detectable signal power S_{min} [11]:

$$R_{max}^4 = \frac{P_t G_A^2 \lambda^2 \sigma}{(4\pi)^3 S_{min}} \quad (1)$$

where P_t is the transmitted power, G_A is the antenna gain, λ the operating wavelength and σ the RCS of the target.

As S_{min} is related to the thermal noise power of the receiver and the required Signal-to-Noise Ratio (SNR_r) to detect a target, the radar equation (1) can be written as follows:

$$R_{max}^4 = \frac{P_t G_A^2 \lambda^2 \sigma}{(4\pi)^3 \cdot kT\Delta f \cdot F \cdot SNR_r} \quad (2)$$

where k is the Boltzmann constant, T the noise temperature in K, Δf the receiver bandwidth in Hz and F its noise factor.

It is important to note that SNR_r is the minimum signal-to-noise ratio at the output of the receiver to ensure the detection of a given target.

In equation (2), the transmitted power and the antenna gain are determined by standardization [2]. The wavelength λ is chosen according to the application and the dimensions of the targets to be detected. The receiver bandwidth Δf is defined by the bandwidth of the front-end filters, which will set the range resolution ΔR of the system ($\Delta R = c/2\Delta f$). The SNR_r is defined by the desired performance in terms of detection and false alarm probabilities. The proposed detection principle is based on frequency and angle variations of the RCS. Thus, the receiver noise factor F is the only adjustable parameter to maximize system performance. Due to the position of the LNA in the receiver chain (see Figure 4), the impact of its noise factor will be more significant over that of the total Radio-Frequency (RF) chain according to the Friis formula:

$$F = F_1 + \frac{F_2 - 1}{G_1} + \frac{F_3 - 1}{G_1 G_2} + ... + \frac{F_n - 1}{G_1 G_2 ... G_{n-1}} \quad (3)$$

where F_i and G_i are the noise factor and the power gain, respectively of the i-th stage, and n is the number of stages.

By setting the objective to detect a cylindrical metal target ($r = 0.6$ cm; $h = 5.4$ cm), up to 2 m at normal incidence, we will determine the required characteristics of the receiver stage and in particular those of the LNA. For this purpose, we extend our system to four bands in 57-66 GHz, distributed around the frequencies 57.8 GHz, 60.2 GHz, 62.8 GHz and 65.2 GHz. The output power of each channel of the $DSPA_2$ is set at 15 dBm (taking into account frequency bands standardization) and the gain of the antennas G_A at 12 dBi (which can be achieved with 4 patches of 6 dBi each). The bandwidth of each frequency channel is 1.6 GHz and the SNR_r depends on the detection technique used. Filter losses are set at 3.5 dB by referring to [12]. In a conventional single-band architecture, the SNR_r to ensure the detection of a nonfluctuating target with a detection probability of 90% and a false alarm probability of 10^{-6} is 13.2 dB [11]. In the case of a multi-band architecture, with a non-coherent integration of 4 pulses from different frequency bands sufficiently spaced, the SNR_r is only 8.3 dB for the same detection and false alarm probabilities. Based on this case of non-coherent integration and using equation (2), we established the technical specifications of the LNA given in Table I, to ensure the targeted detection objective. Reflection coefficients are chosen < -10 dB for an efficient power transfer at input and output of the LNA, otherwise a higher gain will be required.

TABLE I. TECHNICAL SPECIFICATIONS OF THE LNA

Parameters	*Values*
Bandwidth BW	$\geq$ 1.6 GHz
Power gain G	$\geq$ 12.5 dB
Noise figure NF	$<$ 3 dB
S_{11} & S_{22}	< -10 dB

In addition, to determine the predominant parameter of the LNA on the system performance, we studied the influence of its Gain (G) and Noise Figure (NF) on the detection range. This study presented in Table II evaluates the range variations R_V as a function of the variations in G and NF of the LNA. It is based on the following equation obtained by inserting (3) in equation (2):

$$R_{max}^4 = \frac{P_t G_A^2 \lambda^2 \sigma}{(4\pi)^3 \cdot kT\Delta f \cdot SNR_r \cdot \left(NF + \frac{F_f - 1}{G}\right)} \quad (4)$$

where F_f represents the filter losses according to the detection architecture shown in Figure 4.

TABLE II. LNA G AND NF INFLUENCE ON SYSTEM RANGE

G (dB)	*NF (dB)*	*R_V (%)*	*NF (dB)*	*G (dB)*	*R_V (%)*
11-14	2	1.1	2-5	11	16.8
11-14	3	0.9	2-5	12	17.9
11-14	4	0.7	2-5	13	18.2
11-14	5	0.6	2-5	14	18.3

The results show that, on average, a variation of 50% in the noise figure leads to a variation of about 18% in the detection range, while a same variation of 50% in the gain influences only about 1% the range of the system. This demonstrates the overriding of noise figure over gain in improving detection performance particularly in terms of range, as it can be directly seen in equation (4). This result will be very helpful in the choice of the design technology to realize the LNA.

IV. CHOICE OF THE DESIGN TECHNOLOGY

We have two design technologies for the realization of the LNA: SG13S, which is a Bipolar-Complementary Metal Oxide Semiconductor (BiCMOS) SiGe from IHP [13] and D007IH, an m-HEMT GaAs from OMMIC [14]. In order to choose the most suitable technology for the system requirements, we compare them in two steps. The first step focuses on passive elements such as transmission lines (TLs), inductors and capacitors. In the second step, a study of a simple amplifier designed with both technologies is proposed.

The realization of inductances and capacitances becomes more complex as the frequency rises, partly due to increased losses in dielectric substrates and conductors, but also due to coupling effects, which become significant. In order to take these problems into account, we have compared the losses of the TLs and the quality factor (Q-factor) of the grounded TLs, inductors and capacitors. Figure 5 shows a comparison of the losses of the two technologies based on simulations with Advanced Design System (ADS) from Keysight and HFSS. With SG13S technology, Metal1, which is at the lowest metallization level, is chosen as the ground plane. TLs and inductors are made with TopMetal2, which is located at the top level. With D007IH technology, the ground plane is located below the chip. TLs and inductors are made with the metal IN, which is on the top level. The results show a good fit between the ADS and HFSS simulations. They also clearly show that losses are higher with the SG13S (about 0.4 dB/mm more than the D007IH at 60 GHz). Indeed, in the SG13S technology model, there are no losses in the substrate (tangent loss $\tan\delta = 0$). This implies that losses come mainly from conductors. In fact, the ground plane on SG13S is too thin (0.42 μm) compared to 3.5 μm for D007IH. This partly explains the fact that the metal thickness is higher in the SG13S with 3 μm compared to 1.25 μm for D007IH to avoid too much losses. Furthermore, the substrate thickness between the ground plane and the metallization level of the TLs in

the D007IH is nearly ten times greater than the thickness of the substrate between Metal1 and TopMetal2 with SG13S. This results in narrow tracks to make 50 Ω TLs with the SG13S. These different characteristics explain why the losses are higher with SG13S. Finally, this is confirmed by the negative reactance of the TLs characteristic impedance higher in absolute value in SG13S than in D007IH (not shown here).

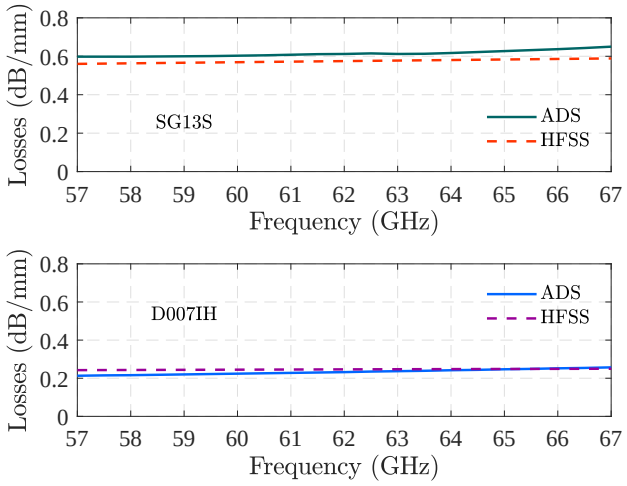

Figure 5. Comparison of 50 Ω TL losses.

A comparison of grounded TLs with the same characteristic impedance of 75 Ω giving rise to an inductance of 0.27 nH at 60 GHz is shown in Figure 6. D007IH exhibits a Q-factor more than 5 times higher than SG13S at 60 GHz.

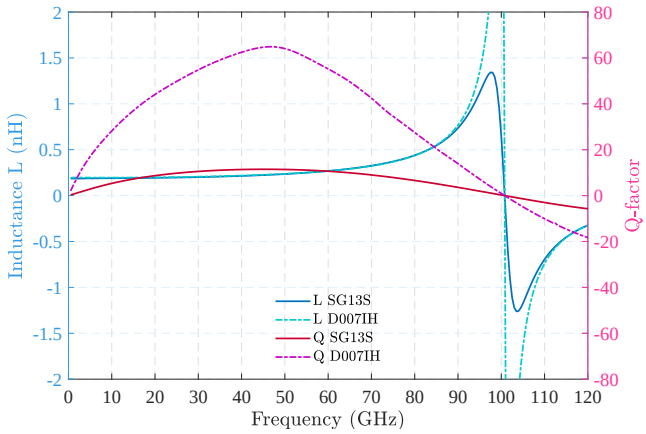

Figure 6. Comparison of grounded TLs.

TABLE III. PASSIVE ELEMENTS PERFORMANCES AT 60 GHz

Parameters	*SG13S*	*D007IH*
50 Ω TL Losses (dB/mm)	0.6	0.22
75 Ω grounded TL Q factor	11	56
1 nH inductance Q factor	14	11
250 fF capacitance Q factor	13	28

The performances of passive elements of the two technologies, based on electromagnetic simulations with ADS Keysight, are summarized in Table III. For the same coil inductor value of 1 nH at 60 GHz, the two technologies have almost equal Q-factor. However, it should be noted that inductors in SG13S are less integrable than those in D007IH because of their shape. For the same capacitor of about 250 fF at 60 GHz, the D007IH has a Q-factor of twice times higher that of the SG13S. On the other hand, for an equivalent surface, the density of a capacitor is higher with SG13S than with D007IH. However, the maximum capacitance value with SG13S is limited to only 8 pF, whereas with D007IH it can achieve 50 pF. As resistors are concerned, we note that the resistance achievable with SG13S are much higher than those possible with D007IH. Resistivities are generally higher on silicon (Si) than on GaAs.

Generally, GaAs technologies have better loss performance than Si technologies. This is partly due to the fact that the resistivity of GaAs substrates is higher than that of Si. Given the characteristics of the passive elements, the SG13S has the advantage of facilitating the realization of more integrable components (lines, capacitors, resistors). On the other hand, it presents too high losses for low noise applications. Unlike SG13S, the D007IH technology has the advantage of having low losses. At 60 GHz, the use of TLs is often preferred for the realization of inductors in particular. Therefore, the D007IH technology, due to its low losses, presents a major advantage for low noise applications. However, at millimeter-wave frequencies, the performance of a circuit does not depend only on the performance of the passive or active elements taken separately. Therefore, an overall analysis of the full circuit elements is necessary. For this reason, we have evaluated the performance of single-stage amplifiers designed with both technologies based essentially on distributed elements and for an operation at 61.5 GHz (see Table IV). The amplifier with

TABLE IV. PERFORMANCE OF SINGLE STAGE AMPLIFIERS

Technology	*Transistor*	*G (dB)*	*NF (dB)*	*P_{DC} (mW)*
SG13S	Bipolar	4.0	2.6	2.0
SG13S	MOS	3.1	2.6	9.2
D007IH	m-HEMT	3.9	1.2	4.1

MOS transistor is the least efficient in terms of gain, NF and power consumption (P_{DC}). The one with bipolar transistor has advantages in terms of gain and power consumption, but its noise figure is high. With the m-HEMT transistor, the amplifier has a gain almost equal to that of the bipolar transistor, with moderate power consumption (more than half that of the MOS transistor), and a noise figure of 1.4 dB lower than that of the bipolar and MOS transistors. Although its reverse isolation (S_{12}) is lower than those of bipolar and MOS transistors, the use of a multi-stage structure will allow to achieve a good level of isolation. Thus, performance with the m-HEMT transistor, with its low noise level, relatively good gain and moderate power consumption seems more suitable to meet our system requirements.

Based on the comparisons made in Tables III and IV, it is clear that the D007IH technology is better suited than the SG13S to meet the required technical specifications set out in Table I, particularly in terms of noise. This is supported by the fact that, regarding to the design, the influence of the LNA noise figure is more significant than that of its gain on the system range. Nevertheless, in order to satisfy the required gain level, the use of a multi-stage structure will be unavoidable.

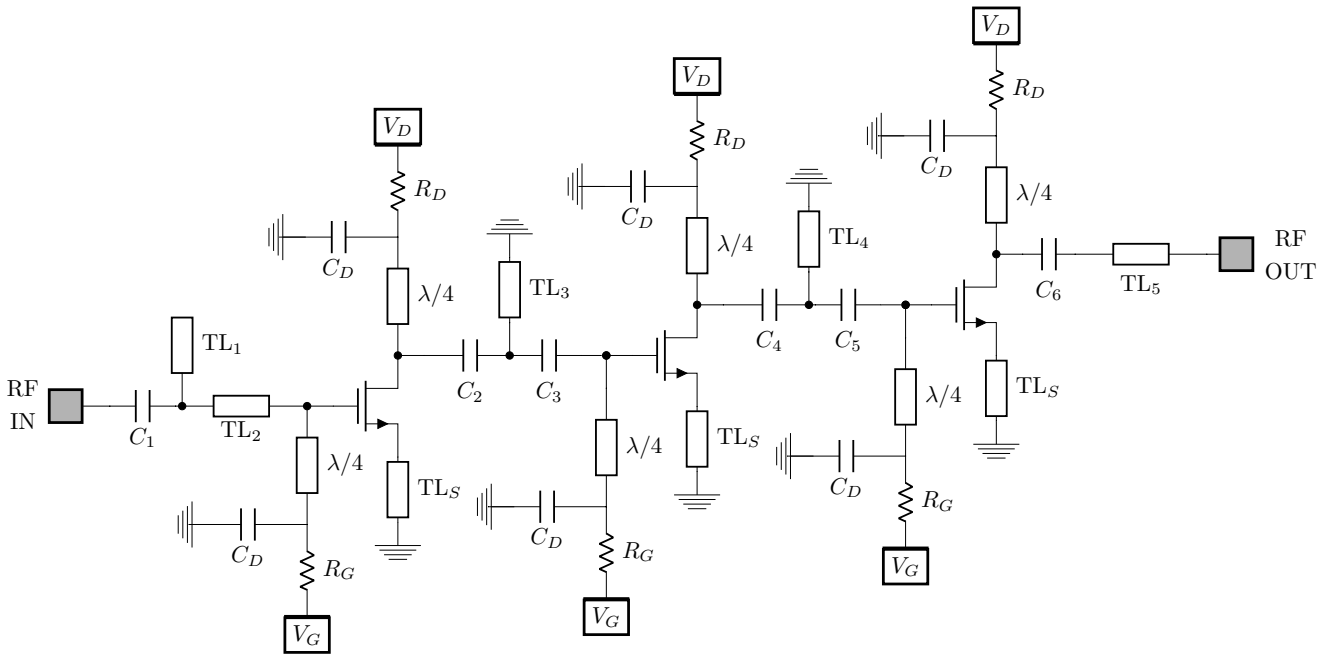

Figure 7. Schematic of the three stages LNA.

D007IH is a 70 nm gate length GaAs technology providing f_T/f_{max} of 300 GHz/450 GHz. It offers a depletion transistor m-HEMT [15], with high transconductance of $g_{m_{max}} = 1600$ mS/mm, which can support a voltage $V_{DS_{max}}$ of 3 V and a maximum current $I_{DSS_{max}}$ of 400 mA/μm. This type of transistor offers good performance in terms of noise, with a noise factor of only 0.5 dB at 30 GHz, giving it a privilege for security applications (millimeter-band imaging), telecommunications or radars. The process of the technology consists of a 3.5 μm metal in its underside, a 100 μm thick GaAs substrate above which different metallization levels are distinguished. These metallization levels are separated by dielectric layers of silicon-nitride (SiN) and silicon-dioxide (SiO_2). The most used metal layer for TLs realization is named IN metal and has a thickness of 1.25 μm. It is also possible to associate this layer with a gold layer of the same thickness for less losses.

V. Design Description of the LNA

The design of the LNA is done with ADS Keysight. Taking into account various simulation tests, the common source topology has been retained. Indeed, this topology is more suitable for low noise components compared to the cascode and common grid topologies [16], the latter offering better stability, higher gain, but also a not desired higher noise figure. In addition, the common source topology is simple to implement and provides moderate gain. In order to meet the required technical specifications of the LNAs established in Table I, particularly in terms of gain, we used a three-stages structure, as shown in Figure 7 [17] [18]. To optimize the performance of an amplifier, transistors size and bias point must be properly chosen. The size of the transistors is selected so as to ensure a good trade-off between gain and noise for the optimal bias point. A parametric study allowed to choose a transistor with 2×25 μm gate development and a voltage $V_{DS} = 1$ V.

The stability of the LNA is ensured by making each stage unconditionally stable. As the transistors are identical for all stages, they are degenerated in the same way so that the overall circuit is unconditionally stable in a larger bandwidth. Figure 8 shows the stability of the first stage through the Rollet's stability factor (K) and the parameter B. In addition, a resistor is used in the bias circuits to further stabilize the LNA. The value of this resistor is meticulously chosen because it influences the gain and noise performance of the LNA [19]. With the voltage drop across the resistor, the V_D potential is increased to 1.1 V to ensure a current $I_{DS} = 4.1$ mA. Moreover, the degeneration of the source allows to closer the Maximum Available Gain (MAG) and NF circles together, as shown in Figure 9. This makes the input stage matching easier [20].

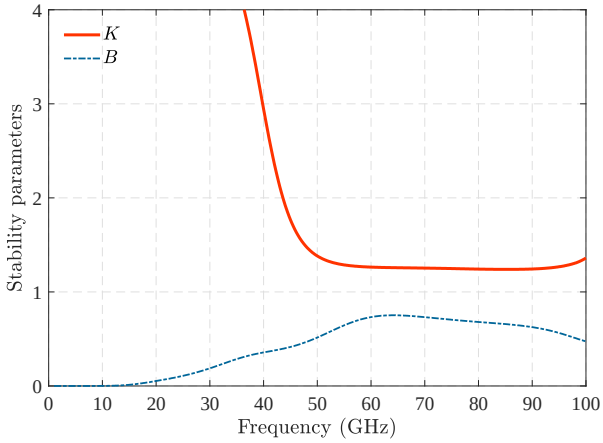

Figure 8. First stage stability.

In Figure 7, each bias circuit is made with a quarter-wave TL, bypass capacitor (C_D) to redirect RF leakage to ground,

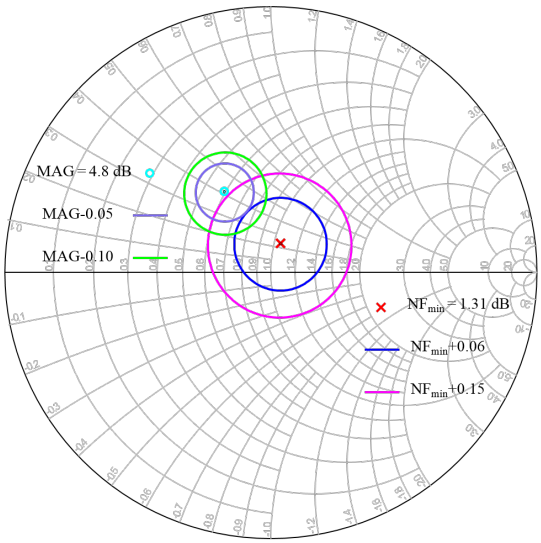

Figure 9. Gain and noise circles for input matching.

and a GaAs implanted resistor (R_G or R_D) to improve low frequency stability. The input matching network is formed by the link capacitor C_1, the open transmission line TL_1, which acts as a capacitor and an inductor made by TL_2. The inter-stages matching networks 1-2 and 2-3 are formed by identical topologies C_2, TL_3, C_3 and C_4, TL_4, C_5 respectively. This topology also makes it possible to isolate the power supplies of the different stages. The output matching is made by a simple serial structure C_6 and TL_5, optimized for a better gain, without too much degradation of the total noise figure of the LNA.

VI. Layout Realization and Simulations Results

At high frequencies and particularly at 60 GHz, the differences between schematic and layout simulations are often significant depending on the accuracy of the passive components models, which is related to the technology. Thus, to minimize these differences, elements such as bias circuits, Direct Current (DC) and RF pads, transistor access and link capacitors have been fixed from their electromagnetic models. This approach allowed the design to be lighter, since only the matching networks will then be optimized during the transition to the full layout.

The layout realization is done progressively in two main steps. Firstly, by considering the results of the partial electromagnetic simulations of the components i.e., each element is simulated alone without taking into account the others. And secondly, the overall simulation of the full LNA circuit. In addition, it should be noted that progressive optimizations have been made in order to maximise the overall performance of the circuit. The resulting 60.2 GHz LNA layout is shown in Figure 10 including RF and DC pads. All TLs are made with the same metal layer denoted IN and ground connections are realized using octagonal vias holes. The size of the circuit is 1.29×1.56 mm^2. Figures 11 and 12 present a comparison between the partial (p-index) and global (g-index) simulations of the LNA. Note that all layout simulations are done with ADS Momentum Microwave solver.

The results show differences related to coupling phenomena between the different elements of the circuit, which are not

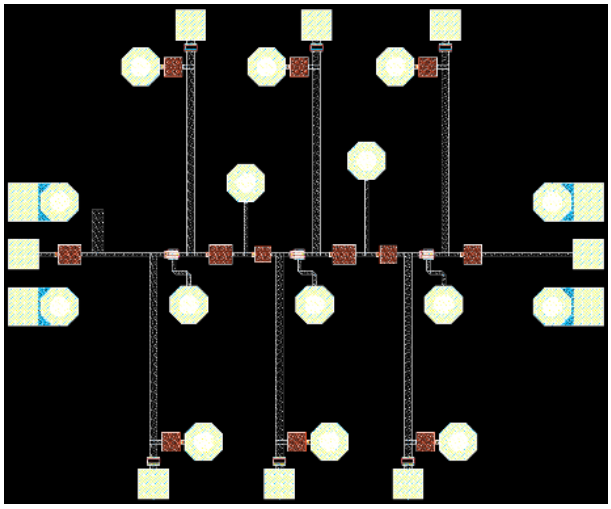

Figure 10. First layout of the LNA.

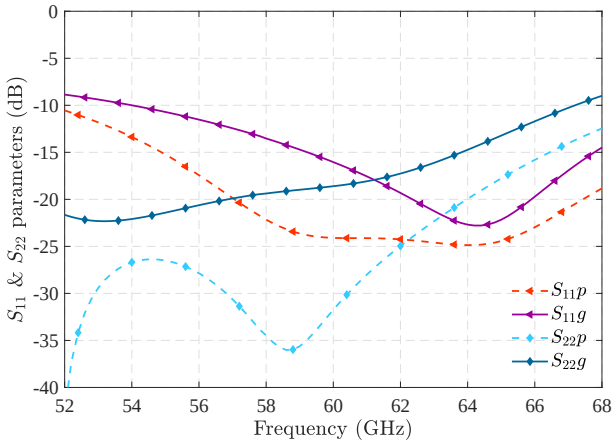

Figure 11. S_{11} and S_{22} with partial and global layout simulations.

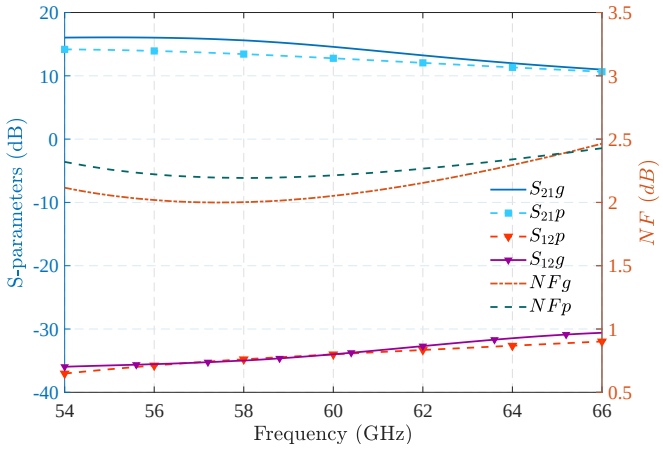

Figure 12. S_{21}, S_{12} and NF with partial and global layout simulations.

taken into account in the partial simulations. These couplings result in a more or less pronounced degradation of the circuit performance. In our case, we can see on Figure 11 the rise in reflection coefficients at both input S_{11} and output S_{22}, but also a slight improvement in the S_{21} coefficient and the noise figure,

as can be seen in Figure 12. In practice, it is very difficult to estimate these couplings. However, a re-optimization has been done to minimize the reflection coefficient degradations, but also to improve as well as possible the gain and noise performances. Moreover, the stability of the circuit is perfectly ensured at least until 100 GHz as shown in Figure 13.

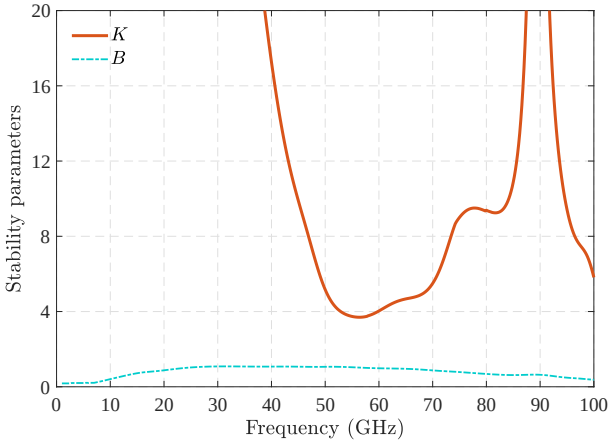

Figure 13. Stability parameters K and B of the whole LNA.

The global simulations results meet the targeted specifications. A gain of 14.5 dB and a noise figure of 2.06 dB are noted at 60.2 GHz. Reverse isolation is approximately -34 dB and the reflexion coefficients S_{11} and S_{22} are less than -15 dB in the band of interest (59.4-61 GHz). The -3 dB bandwidth (for $S_{11} < -10$ dB and $S_{22} < -10$ dB) ranges from 54 to 65 GHz with a fluctuation of about 0.38 dB in noise figure. In the band of interest, the variation in gain is about 0.9 dB and the noise figure ripple is less than 0.1 dB. In addition, the LNA consumes about 13.5 mW.

VII. Design Optimization and Characterization

To gain in miniaturization, we have optimized the size of the LNA. This is done progressively in two main steps. We started by reducing the length of the bias circuits so that the LNA does not exceed 1 mm following to the height of Figure 10. This was done by replacing the straight quarter-wave TLs by equivalent meandered lines. The use of meandered lines more or less changes the impedances presented at the input and output of the transistors. Therefore, the matching networks have been re-optimized. Thus, the capacitors and the grounded TLs have been resized in order to reduce the overall size of the circuit while minimizing the potential coupling between circuit elements. This made it possible to limit the rise in coefficients (S_{11} and S_{22}) and to guarantee the required performance in terms of gain and noise. The optimized LNA is shown in Figure 14 and occupies an area of 1.0×1.47 mm^2. Its S-parameters and noise figure are shown in Figure 15 and the non-linear characteristics in Figures 16 and 17.

Table V presents a comparison of the LNA performance before and after optimization in the band of interest for the detection system. With a gain of 14.3 dB and a noise figure of 2.1 dB at 60.2 GHz, the optimized LNA has almost identical performances with the one shown in Figure 10. The reflexion coefficients are less than -15.4 dB for S_{11} and -16.3 dB for S_{22} in the band of interest. Also note that the stability of the LNA

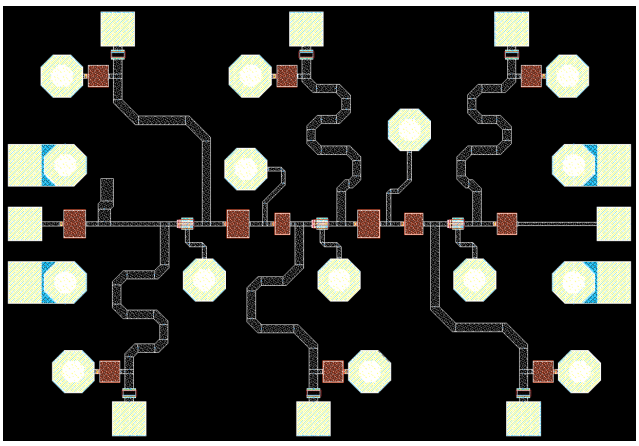

Figure 14. Layout of the optimized LNA.

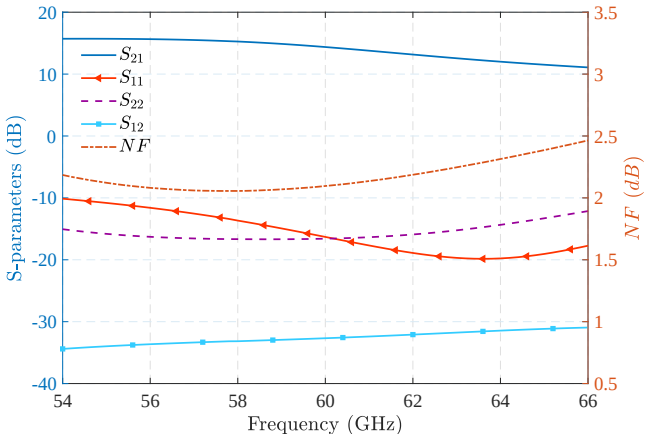

Figure 15. S-parameters and noise figure.

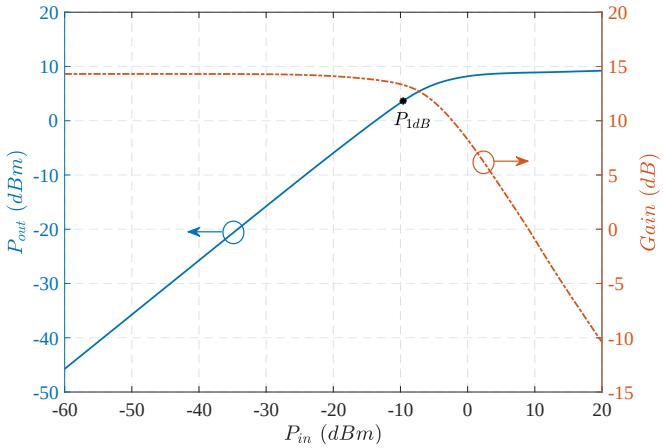

Figure 16. Gain and 1 dB compression point.

has been verified, and as before optimization, unconditional stability is ensured up to at least 100 GHz. The non-linear characteristics show good performances with a very slight improvement form -10 dBm to -9.6 dBm for the IP_{1dB} and from -4.4 dBm to -3.9 dBm for the $IIP3$. All of the above mentioned results prove a meticulous optimization of the LNA with an area reduction of about 27% , while maintaning the same power consumption of 13.5 mW.

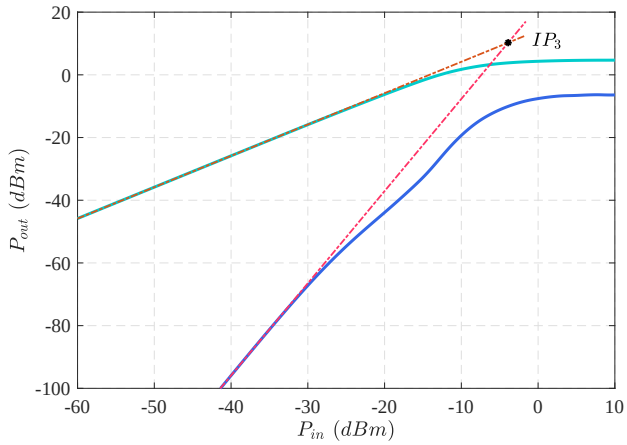

Figure 17. Third order interception point (IP3).

TABLE V. FEATURES OF THE OPTIMIZED LNA IN 59.4-61 GHz

Parameters	*First LNA*	*Optimized LNA*
S_{21} (dB)	14.5 ± 0.045	14.3 ± 0.4
NF (dB)	2.06 ± 0.03	2.10 ± 0.03
S_{11} (dB)	< -15.2	< -15.4
S_{22} (dB)	< -18	< -16.3
S_{12} (dB)	< -33.3	< -32.4
IP_{1dB} (dBm)	-10	-9.6
$IIP3$ (dBm)	-4.4	-3.9
Area (mm^2)	1.29×1.56	1.0×1.47

To further characterize our design, we are now evaluating its sensitivity to bias voltages, temperature and load variations in the band of interest (59.4-61 GHz). These studies are necessary to see how these parameters will influence the performance of the designed LNA and more globally the performance of the system.

Voltage sensitivity is evaluated by quantifying the variations in S_{21} and NF following the bias voltages V_{DS} and V_{GS} variations respectively, depending on whether their influences are more or less significant. Results are shown in Figures 18 and 19 with a variation of ± 10 % around the nominal bias voltage. The results of these studies show that our circuit is not very sensitive to bias voltage errors. Indeed, a 20% variation in the V_{GS} voltage leads to a variation of about 2 dB in gain

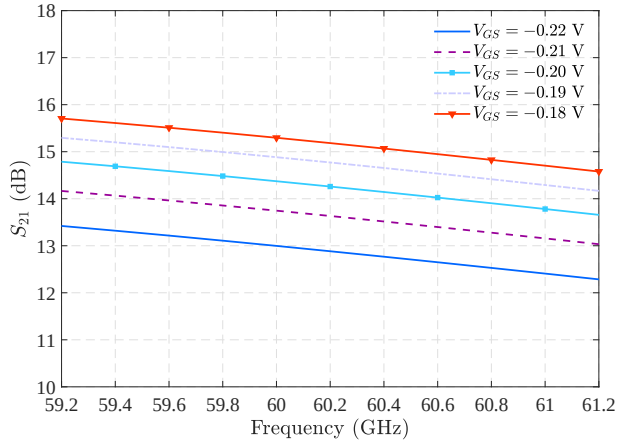

Figure 18. S_{21} sensitivity to bias voltage.

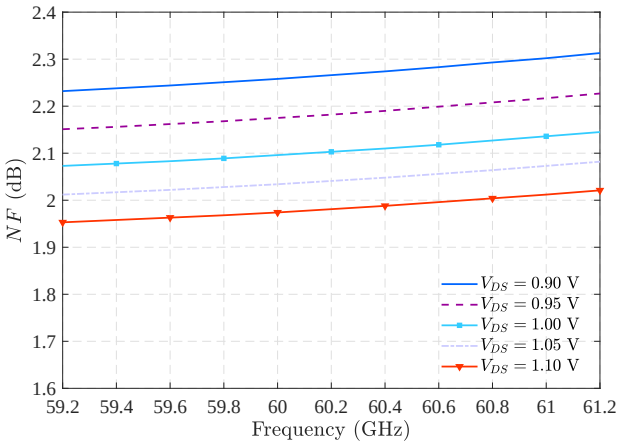

Figure 19. NF sensitivity to bias voltage.

(< 50 %), which has a negligible influence on the range of the system (see Table II). On the other hand, a 20% variation of the V_{DS} leads to a fluctuation of less than 0.3 dB in the noise figure. This corresponds to a variation of less than 1%, thus a negligible influence on the system range as it can be deduced from Table II.

Usually, the simulation temperature is taken at $16.85°$ C (290 K) as recommended by the IEEE standard for noise figure measurements. Thus, to characterize the temperature sensitivity of the LNA, we have simulated it under different temperatures ranging from $-40°$ C to $125°$ C. The results obtained in noise figure variations are shown in Figure 20. Gain variations are not presented here, because they are obviously negligible (< 0.1 dB). The results show a maximum variation of 0.24 dB in the noise figure between 59.4-61 GHz. As with the voltage sensitivity, these results show a negligible influence of noise figure variations on the system range when the LNA is subjected to large temperature variations.

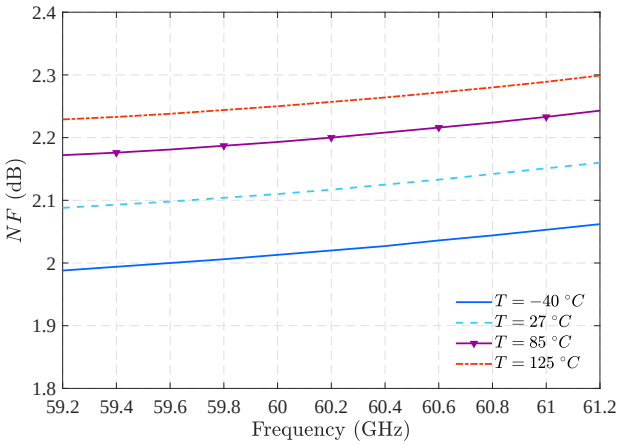

Figure 20. NF sensitivity to temperature.

After voltage and temperature, it seems particularly significant in the configuration of the detection architecture to study the influence of the impedance mismatch at the LNA input. In other words, it means seeing the influence of the antenna impedance with respect to that of the LNA input. To do this, we evaluated the variations in gain and noise figure of the LNA

TABLE VI. PERFORMANCE COMPARISON

Ref.	*Technology*	*Freq. (GHz)*	*G (dB)*	*NF (dB)*	*IP_{1dB} (dBm)*	*IIP3 (dBm)*	*P_{DC} (mW)*	*FoM_N*	Area (mm^2)
[4]	130 nm SiGe BiCMOS*	57-66	20.5	4.3	-17.8	-11,1	9.8	0.51	0.41 x 0.32
[19]	100 nm GaAs m-HEMT$^+$	60-90	19	2.5	-	-	56	0.20	3.5 x 1.0
[21]	40 nm CMOS$^+$	60	12.5	3.8	-	-15	20.4	0.30	0.63 x 0.31
[22]	65 nm CMOS$^+$	60	23	4	-26	-	8	0.70	0.35 x 0.14
[23]	90 nm CMOS$^+$	58-77	11.2	4.8	-18.7	-7.4	10	0.41	0.72 x 0.76
[24]	65 nm CMOS$^+$	60	20.2	5.2	-25	-	28	0.13	0.54 x 0.80
[25]	65 nm CMOS*	61	22	5.5	-	-10.7	26	0.13	0.71 x 0.46
[26]	130 nm SiGe BiCMOS+	52-56	15	3.3-3.6	-13.5	-	19.6	0.37	0.30 x 0.35
[27]	50 nm GaAs m-HEMT$^+$	60-90	27	2.6	-26	-	45	0.23	1.6 x 2.3
This work	**70 nm GaAs m-HEMT***	**60**	**14.3**	**2.1**	**-9.6**	**-3.9**	**13.5**	**1.0**	**1.47 x 1.0**

$^+$ Measures
$*$ Simulations

by changing its input impedance with a $\pm 10\%$ variation around the nominal value of 50 Ω, as shown in Figure 21. The results show that both the gain and the noise figure have a fluctuation of less than 0.1 dB when the input impedance of the LNA is varied from 45 Ω to 55 Ω. Again, the performance of the LNA shows negligible variations that will not have significant influence on the detection system range.

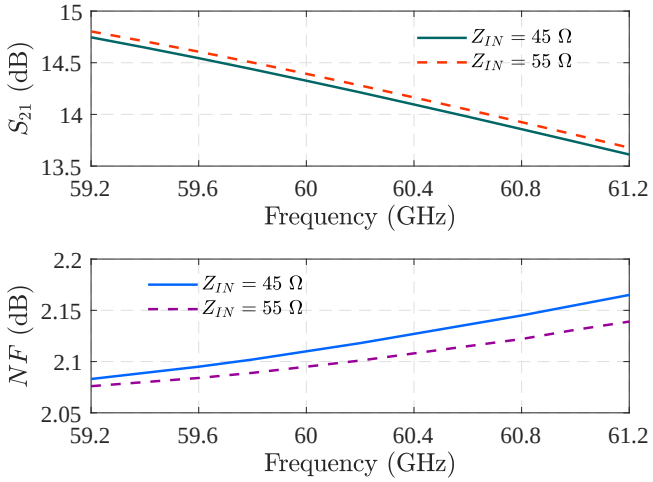

Figure 21. S_{21} and NF sensitivity to input impedance Z_{IN}.

Concisely, sensitivity studies reveal a high robustness of the designed LNA with respect to variations in bias voltage, temperature and input load (mismatch). In fact, in all three cases, the maximum variation in gain is about 2 dB for a variation of $\pm 10\%$ in V_{GS} voltage, while for the noise figure it is less than 0.3 dB. These sensitivity performances avoid a significant decrease of the system range when the LNA is subjected to significant variations in voltage, temperature or input load.

Finally, the performance of the designed LNA compared with the state-of-the-art is summarized in Table VI. LNAs designed around 60 GHz with different technologies are considered. Usually, the figure of merit (FoM) of an LNA is calculated as a function of the gain, noise figure and power consumption as defined in [3]. But, considering that the influence of the gain is negligible on the detection performance of the system (particularly in terms of range, as shown in Table II), we define the FoM as follows:

$$FoM = \frac{1}{(NF - 1) \cdot P_{DC}} \tag{5}$$

This definition of the FoM is more consistent to our detection context, especially in relation to the proposed architecture. Furthermore, it should be noted that in Table VI, the FoM_N is the normalized FoM to our LNA result. Regarding Table VI, our LNA shows good performance, especially in terms of noise figure, even if some of the results are based on measurements. With a moderate power consumption compared to other III-V technologies [19] and [27] or even the 40 nm CMOS [21], it presents a good gain and meet the targeted detection objectives. Note that more gain can be achieved by increasing the drain voltage of the output stage or adding a fourth transistor. But this would obviously increase the power consumption and a little more the noise figure. In addition, it is clear that the non-linear characteristics of our designed LNA are much better than those of the m-HEMT and CMOS technologies presented in Table VI. As an example, its IP_{1dB} is -9.6 dBm, while it is less than -17 dBm for [4] [22]- [24] and [27]. The same is observed for the $IIP3$. Moreover, our LNA is more integrable compared to the reported same type technologies (50 and 100 nm GaAs m-HEMT). In our detection context, our design is more efficient with a better figure of merit.

In summary, the performance of the designed LNA satisfy perfectly the specifications established in Table I. Furthermore, with these performances and taking into account the proposed system (see Figure 4), the detection range is improved up to 2.3 m for the considered metal cylinder ($r = 0.6$ cm; $h = 5.4$ cm) at normal incidence ($\theta = 0°$), when a non-coherent integration is performed over the received signals in the four frequency bands. This represents an improvement of 30% in range compared to a conventional single-band detection system.

VIII. Conclusion and Future Work

This work focused on the design of a 60 GHz LNA for small metal objects detection system. Firstly, the detection principle was presented with an impulse architecture based on frequency channel diversity. Starting from the radar equation and targeted detection objectives, the critical components of the architecture were identified and the required LNAs specifications established. Following this, the design technology was choosen based on a comparative study between BiCMOS SiGe and m-HEMT GaAs. Then, the design was done in a 70 nm GaAs m-HEMT technology from OMMIC. Three stages transistors with inductive degeneration and bias circuits including resistance were used to better scale the transistor with a good trade-off between gain and noise, while ensuring unconditionnal stability up to 100 GHz. The LNA is completed with ADS Keysight. Critical design issues related to coupling phenomena were highlighted. Post-layout simulation results with ADS Momentum Microwave solver show good performance, especially in terms of noise. With a noise figure of 2.1 dB at 60 GHz, our LNA is much better that those commonly found in the state-of-the-art. For a moderate power consumption of 13.5 mW, which is relativeley low for III-V's technologies, it exhibits 14.3 dB of gain at 60 GHz. The reflection coefficients are less than -10 dB in the 54-68 GHz band. The LNA shows an input power at 1 dB compression point of -9.6 dBm and an input third order interception point of -3.9 dBm. Furthermore, the designed LNA occupies less space with 1.0×1.47 mm^2 compared to others of the same type of technology. In addition, it has been characterized in terms of sensitivity to voltage biasing, temperature and input impedance variations. This characterization shows good robustness of the design. At the end, it was compared to other recently published 60 GHz LNAs, particularly with a specific figure of merit adapted to our detection context. The results of our design show the potential of III-V's technologies, especially the 70 nm GaAs m-HEMT for very low noise applications, particularly to improve the performance of detection systems.

In terms of design, some future work is planned. First, we have the manufacturing and characterization by measurements. And in a longer term, the joint design of the reception chain (i.e., LNA, filter and detector) to further improve the system performances.

References

[1] P. S. Diao, T. Alves, B. Poussot, and M. Villegas, "60 GHz Low-Noise Amplifier in a 70 nm GaAs m-HEMT Technology for Multi-band Impulse Detection System," in Proceedings of the 12th International Conference on Advances in Circuits, Electronics and Micro-electronics (CENICS) Oct. 27–31, 2019, Nice, France. IARIA, 2019, pp. 19–24.

[2] M. G. L. Frecassetti, "E-Band and V-Band-Survey on status of world-wide regulation," ETSI White Paper, no. 9, June 2015, pp. 1–40.

[3] A. C. Ulusoy et al., "A SiGe D-Band Low-Noise Amplifier Utilizing Gain-Boosting Technique," IEEE Microwave and Wireless Components Letters, vol. 25, no. 1, 2015, pp. 61–63.

[4] M. Pallesen, "Design of a 60 GHz Low Noise Amplifier in a 0.13 μm SiGe BiCMOS Process," Master's thesis, The University of Bergen, 2016, URL: http://bora.uib.no/handle/1956/12595 [accessed: 2017-10-24].

[5] A. Dyskin, D. Ritter, and I. Kallfass, "Ultra wideband cascaded low noise amplifier implemented in 100-nm GaAs metamorphic-HEMT technology," in Proceedings of the International Symposium on Signals, Systems, and Electronics (ISSSE) Oct. 3–5, 2012, Potsdam, Germany. IEEE, Dec. 2012, pp. 1–4.

[6] Y. Chen et al., "OMMIC 70 nm mHEMT LNA design," in Proceedings of the IEEE Asia Pacific Microwave Conference (APMC) Nov. 13–16, 2014, Kuala Lumpar, Malaysia. IEEE, Jan. 2018, pp. 1192–1195.

[7] P. S. Diao, T. Alves, B. Poussot, and M. Villegas, "A new method and transceiver architecture dedicated to continuous detection of very small metallic object," in Proceedings of the 10th Global Symposium on Millimeter-Waves (GSMM) May 24–26, 2017, Hong Kong, China. IEEE, Jul. 2017, pp. 169–171.

[8] D. K. Barton, Frequency Diversity Theory. Artech House Inc., 1977, vol. 6 of Radars, section 2, pp. 35–114, in Frequency Agility and Diversity, ISBN: 0-89006-067-3.

[9] P. S. Diao, T. Alves, M. Villegas, and B. Poussot, "Compact millimeter wave architecture dedicated to object detection using dual band-dual polarization and impulse method," in Proceedings of the 13th Conference on Ph.D. Research in Microelectronics and Electronics (PRIME) June 12–15, 2017, Giardini Naxos, Italy. IEEE, Jul. 2017, pp. 161–164.

[10] P. Surendran, J.-H. Lee, and S. J. Ko, Performance of Non-coherent Detectors for Ultra Wide Band Short Range Radar in Automobile Applications. Springer-Verlag Berlin Heidelberg, 2012, vol. 377, pp. 185–195 in Software Engineering Research, Management and Applications 2011, ISBN: 978-3-642-23201-5.

[11] M. I. Skolnik, The Radar Equation, 2nd ed. McGraw Hill, Inc., 1980, chapter 2, pp. 15–67, in Introduction to Radar Systems, ISBN: 0-07-057909-1.

[12] R. Abdaoui, M. Villegas, G. Baudoin, and A. Diet, "Microstrip band pass filter bank for 60 GHz UWB impulse radio multi band architectures," in Proceedings of the IEEE MTT-S International Microwave Workshop Series on Millimeter Wave Integration Technologies Sep. 15–16, 2011, Sitges, Spain. IEEE, Oct. 2011, pp. 192–195.

[13] "SG13S Process Specification Rev. 1.06," July 2016, URL: https://www.ihp-microelectronics.com/en/services/mpw-prototyping/sigec-bicmos-technologies.html [accessed: 2017-10-18].

[14] "D007IH Design Manual - OM-CI/008/MG," Oct. 2017, URL: http://www.ommic.fr/site/mpw-4r [accessed: 2018-07-20].

[15] M. Ney, HEMT's capability for millimeter wave applications. Hermes Penton Science, 2002, chapter 2, pp. 20–42, in Millimeter Waves in Communication Systems, ISBN: 19039 9617 1.

[16] T. Das, "Practical Considerations for Low Noise Amplifier Design," RFLNA White Paper Rev. 0, Freescale Semiconductor, Inc., May 2013, pp. 1–9.

[17] P. S. Diao, T. Alves, B. Poussot, and M. Villegas, "A 60 GHz Low-Noise Amplifier for Detection Systems," in Proceedings of the 2019 IEEE Radio and Antenna Days of the Indian Ocean (RADIO) Sep. 23–26, 2019, Reunion. IEEE, Jan. 2020, pp. 1–2.

[18] P. S. Diao, "60 GHz Low-Noise Amplifier for Detection Systems," IOP Conference Series: Materials Science and Engineering, vol. 766, Mar. 2020, p. 012003.

[19] A. Bessemoulin, J. Grunenputt, P. Felton, A. Tessmann, and E. Kohn, "Coplanar W-band low noise amplifier MMIC using 100-nm gate-length GaAs PHEMTs," in Proceedings of the 34th European Microwave Conference Oct. 12–14, 2004, Amsterdam, The Netherlands, vol. 1. IEEE, 2005, pp. 25–28.

[20] S. P. Voinigescu et al., "A scalable high-frequency noise model for bipolar transistors with application to optimal transistor sizing for low-noise amplifier design," IEEE Journal of Solid-State Circuits, vol. 32, no. 9, 1997, pp. 1430–1439.

[21] H. Gao et al., "A 48–61 GHz LNA in 40-nm CMOS with 3.6 dB minimum NF employing a metal slotting method," in Proceedings of the IEEE Radio Frequency Integrated Circuits Symposium (RFIC) May 22–24, 2016, San Francisco, CA, USA. IEEE, Jul. 2016, pp. 154–157.

[22] E. Cohen, O. Degani, and D. Ritter, "A wideband gain-boosting 8 mW LNA with 23 dB gain and 4 dB NF in 65 nm CMOS process for 60 GHz applications," in Proceedings of the IEEE Radio Frequency Integrated Circuits Symposium June 17–19, 2012, Montreal, QC, Canada. IEEE, Jul. 2012, pp. 207–210.

[23] Y.-S. Lin, C.-Y. Lee, and C.-C. Chen, "A 9.99 mW low-noise amplifier for 60 GHz WPAN system and 77 GHz automobile radar system in 90 nm CMOS," in Proceedings of the IEEE Radio and Wireless Symposium (RWS) Jan. 25–28, 2015, San Diego, CA, USA. IEEE, 2015, pp. 65–67.

[24] C. So and S. Hong, "60 GHz variable gain LNA with small NF variation," in Proceedings of the IEEE International Symposium on Radio-Frequency Integration Technology (RFIT) 30 Aug.–1 Sep., 2017, Seoul, South Korea. IEEE, Sep. 2017, pp. 171–173.

[25] A. Wang, L. Li, and T. Cui, "A transformer neutralization based 60 GHz LNA in 65 nm LP CMOS with 22 dB gain and 5.5 dB NF," in Proceedings of the IEEE International Symposium on Circuits and Systems (ISCAS2013) May 19–23, 2013, Beijing, China. IEEE, Aug. 2012, pp. 1111–1114.

[26] S. Zihir and G. M. Rebeiz, "A wideband 60 GHz LNA with 3.3 dB minimum noise figure," in Proceedings of the IEEE MTT-S International Microwave Symposium (IMS) June 4–9, 2011, Honololu, HI, USA. IEEE, Oct. 2017, pp. 1969–1971.

[27] P. M. Smith et al., "A 50 nm mHEMT millimeter-wave MMIC LNA with wideband noise and gain performance," in Proceedings of the IEEE MTT-S International Microwave Symposium (IMS2014) June 1–6, 2014, Tampa, FL, USA. IEEE, Jul. 2014, pp. 1–4.